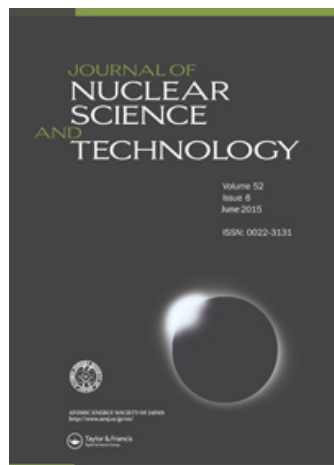


This article was downloaded by: [CEA Cadarache]

On: 17 May 2015, At: 13:59

Publisher: Taylor & Francis

Informa Ltd Registered in England and Wales Registered Number: 1072954 Registered office: Mortimer House, 37-41 Mortimer Street, London W1T 3JH, UK



## Journal of Nuclear Science and Technology

Publication details, including instructions for authors and subscription information:

<http://www.tandfonline.com/loi/tnst20>

### Light and heavy water dynamic structure factor for neutron transport codes

Emmanuel Farhi<sup>a</sup>, Ghislain Ferran<sup>b</sup>, Wim Haeck<sup>b</sup>, Eric Pellegrini<sup>a</sup> & Yoann Calzavara<sup>a</sup>

<sup>a</sup> Institut Laue Langevin, BP156, 38042 Grenoble, France

<sup>b</sup> Institut de Radioprotection et de Sûreté Nucléaire, PSN-EXP/SNC/LNR, Fontenay-aux-Roses, France

Published online: 24 Nov 2014.



[Click for updates](#)

To cite this article: Emmanuel Farhi, Ghislain Ferran, Wim Haeck, Eric Pellegrini & Yoann Calzavara (2015) Light and heavy water dynamic structure factor for neutron transport codes, Journal of Nuclear Science and Technology, 52:6, 844-856, DOI: [10.1080/00223131.2014.984002](https://doi.org/10.1080/00223131.2014.984002)

To link to this article: <http://dx.doi.org/10.1080/00223131.2014.984002>

PLEASE SCROLL DOWN FOR ARTICLE

Taylor & Francis makes every effort to ensure the accuracy of all the information (the "Content") contained in the publications on our platform. However, Taylor & Francis, our agents, and our licensors make no representations or warranties whatsoever as to the accuracy, completeness, or suitability for any purpose of the Content. Any opinions and views expressed in this publication are the opinions and views of the authors, and are not the views of or endorsed by Taylor & Francis. The accuracy of the Content should not be relied upon and should be independently verified with primary sources of information. Taylor and Francis shall not be liable for any losses, actions, claims, proceedings, demands, costs, expenses, damages, and other liabilities whatsoever or howsoever caused arising directly or indirectly in connection with, in relation to or arising out of the use of the Content.

This article may be used for research, teaching, and private study purposes. Any substantial or systematic reproduction, redistribution, reselling, loan, sub-licensing, systematic supply, or distribution in any form to anyone is expressly forbidden. Terms & Conditions of access and use can be found at <http://www.tandfonline.com/page/terms-and-conditions>

## ARTICLE

### Light and heavy water dynamic structure factor for neutron transport codes

Emmanuel Farhi<sup>a\*</sup>, Ghislain Ferran<sup>b</sup>, Wim Haeck<sup>b</sup>, Eric Pellegrini<sup>a</sup> and Yoann Calzavara<sup>a</sup>

<sup>a</sup>Institut Laue Langevin, BP156, 38042 Grenoble, France; <sup>b</sup>Institut de Radioprotection et de Sûreté Nucléaire, PSN-EXP/SNC/LNR, Fontenay-aux-Roses, France

(Received 19 August 2014; accepted final version for publication 31 October 2014)

In this study, we report on recent neutron inelastic scattering experiments performed at the Institut Laue-Langevin (ILL) for H<sub>2</sub>O and D<sub>2</sub>O. The measured dynamic structure factors  $S(q, \omega)$  have been reduced, normalised and transformed into the  $S(\alpha, \beta)$  formalism, where  $\alpha$  and  $\beta$  stand for the unit-less momentum and energy transfers, respectively. The measurements were complemented with molecular dynamics simulations. After processing with NJOY, new water neutron scattering cross-sections have been generated for use with e.g. the Monte Carlo N-Particle (MCNP) software in view to improve the accuracy of the nuclear facility models. As an example, we present improved accuracy calculations for the safety rod insertion impact on the criticality factor  $k_{\text{eff}}$  for the ILL high flux research reactor.

**Keywords:** water; cross-sections; double differential cross-section; neutron; criticality; nuclear reactor; dynamic structure factor; ENDF/B-VI; MCNP; neutron nuclear data

#### 1. Introduction

One caveat of the neutron cross-section libraries for reactor physics (ENDF, JEFF, JENDL, etc.) is the evaluation process of the thermal neutron cross-sections in liquids, especially in hydrogenated liquids. The present data [1] may actually lead to significant discrepancies between measurements and calculations when modelling e.g. thermal neutrons in water (light and heavy). Recent studies based upon international benchmarks [2,3] highlighted the strong dependency of the reactor calculation validity on the thermalisation process treatment. This may be explained by the numerous approximations used for the evaluation of the thermal cross-sections for light and heavy water, even when using the most recent libraries such as JEFF3.2 and ENDF/B-VII.1 [4–6].

The sensibility of the calculation results on the thermal neutron cross-sections is particularly obvious for heavy water because of the weak absorption and the high scattering power of deuterium. But, as opposed to light water, heavy water cannot be considered as a pure incoherent scatterer. This phenomenon can thus be observed when modelling a heavy water moderated reactor such as the Institut Laue-Langevin (ILL) High Flux Reactor, Grenoble, France. In this case, the quality of the nuclear reactor modelling can be estimated by the behaviour of the multiplication factor,  $k_{\text{eff}}$ , which cannot be reproduced in a totally satisfactory way when introducing the

safety rods (SR) in this reactor with current thermal water cross-sections values [7]. Moreover, the sensibility of the  $k_{\text{eff}}$  assessment on the thermal neutron cross-sections may also be observed for light water systems [8]. The consequences on reactor physics and criticality studies can be significant in such cases. Furthermore, the tabulated values are today only available for a small amount of temperatures, which strongly limits their use both for research and industrial applications.

We believe that the libraries accuracy could be enhanced by the direct introduction of measured dynamic structure factors  $S(q, \omega)$ , where  $q$  is the neutron momentum transfer and  $\omega$  is the neutron energy transfer. Indeed, until now all evaluations related to thermal neutron are based upon experiments performed with a momentum transfer  $q \rightarrow 0$ , like infrared (IR) or Raman (the ‘frequency spectrum’). The extension on the whole momentum domain is carried out by approximate laws [9] which take as input the vibrational density of states (DOS) of modes and tend to ignore fine structure and dynamics features in the material. This is actually the case even for the most recent libraries, the accuracy of which remains poor for the slowest neutrons [6,10–12]. This approximation is unsatisfactory to us, especially for liquids such as water.

Most neutron cross-sections available from libraries are generated by the LEAPR module of NJOY. The

\*Corresponding author. Email: farhi@ill.fr

LEAPR module of NJOY [1] can handle many scattering processes in materials. The inelastic scattering terms are described as a set of vibrational frequencies, which are fully adapted to non-dispersive modes such as intramolecular, vibrational, rotational and quantum lines. The phonon expansion also considers a set of discrete oscillators at given frequencies. That is why LEAPR usually requires as input the frequency spectrum (DOS) of the material, which is decomposed as a set of distinct vibrational modes. For large momentum values, the short collision time approximation is used, which models all materials as incoherent scatterers, basically  $S(q, \omega)$  is a Gaussian, shifted by the recoil energy. A diffusive model can be used to describe a liquid, and usually produces a quasi-Lorentzian  $S(q, \omega)$ . The incoherent elastic scattering is computed as a single exponential decay on the elastic line. Last, the coherent elastic scattering can account for discrete structural peaks, as found in crystals and powders, but only makes use of it to compute the total scattering cross-section (which exhibits Bragg edges). All of these processes are treated as separate, analytical methods which add up to provide the total scattering cross-section. Specific models have been developed to describe the hydrogen and deuterium cryogenic liquid, used as neutron cold moderators.

We expect that fully taking into account the measurements of the scattering function  $S(q, \omega)$  may enable to lower the impact of the extension law approximations cited above [9] and thus to significantly enhance the accuracy of the neutron cross-section estimates. For this reason, we carried out recent neutron inelastic scattering experiments on neutron spectrometers at the ILL. Measured dynamic structure factors  $S(q, \omega)$  for light and heavy water have been treated, normalised and transformed in the  $S(\alpha, \beta)$  formalism, where  $\alpha$  and  $\beta$  are relevant for the unit-less momentum and energy transfers, respectively. The measurements were completed by molecular dynamics (MD) simulations in order to extend the applicable dynamic range. Thanks to this formalism, the treated data can be processed by the code NJOY (directly by the THERMR sub-code) [1] in the ACER format for instance. It is then possible to run the Monte Carlo N-Particle (MCNP) software calculations taking fully into account these experimental data.

We present here the method used to implement measured thermal neutron cross-sections into MCNP, as well as a usage example demonstrating the accuracy improvement which can be expected from this new data.

## 2. Structure and dynamics of water: neutron scattering measurements and molecular dynamics

Following Squires [13], the experimental counterpart of the scattering law  $S(q, \omega)$  is the neutron double differential scattering cross-section for both coherent and incoherent processes:

$$\frac{d^2\sigma}{d\Omega dE_f} = \frac{\sigma}{4\pi} \frac{k_f}{k_i} N S(q, \omega), \quad (1)$$

which describes the number of neutrons scattered per unit solid angle  $d\Omega$  and per unit final energy  $dE_f$ . In this equation,  $N = \rho V$  is the number of scattering units (atoms or molecules) in the scattering volume  $V$  with atomic/molecular number density  $\rho$ ,  $E_f$ ,  $E_i$ ,  $k_f$ ,  $k_i$  are the kinetic energies and wave-vectors of the final and initial states, respectively,  $\sigma$  is the bound atom/molecule scattering cross-section,  $\Omega$  is the solid angle and  $q, \omega$  are the wave-vector and energy transfer at the sample, so that  $\hbar\vec{q} = \vec{k}_i - \vec{k}_f$  and  $\hbar\omega = E_i - E_f$ . In general, the total dynamic structure factor can be written as the sum of the coherent and the incoherent (or self) scattering cross-section contributions,  $\sigma S(q, \omega) = \sigma_{\text{coh}} S_{\text{coh}}(q, \omega) + \sigma_{\text{inc}} S_{\text{inc}}(q, \omega)$ . In non mono-atomic liquids, such as water, the coherent  $S_{\text{coh}}$  and incoherent  $S_{\text{inc}}$  scattering laws are computed from sums of partial contributions  $S_{ij}$ , where  $i$  and  $j$  represent atoms in the material, weighted by their respective scattering length  $b_i$  and  $b_j$ .

In the following, we present new neutron scattering dynamic structure factor measurements and MD results. Then, we characterise these results with inferred structural and dynamical quantities, which we compare with previous studies. Having validated our results, we merge experimental and simulated data-sets, in view to combine them with the existing ENDF tables. It is not our purpose here to develop further the discussion about the structure of water molecules, nor their dynamical properties, but only to show how we can use that data to improve the quality of the nuclear databases.

### 2.1. Neutron scattering measurements

Conversely, the dynamic structure factor can directly be extracted from the measured scattered intensity on e.g. an inelastic neutron scattering spectrometer with large detectors.

In order to extract the total scattering function  $S$ , we have carried out experiments at the ILL, Grenoble, France. For this purpose, we have used two state-of-the-art time-of-flight spectrometers, IN4 and IN5, of which the geometry is shown in **Figure 1**. The total measurement time was one day per instrument.

The IN4 instrument is a direct geometry crystal neutron time-of-flight spectrometer used for the study of excitations in condensed matter [14]. The incoming neutron beam from the ILL reactor is monochromatised and pulsed after passing two background choppers, a pyrolytic graphite double curvature focusing monochromator and a fast Fermi chopper. A radial collimator around the sample position is used to cut the scattering from the sample environment. The scattered signal from the sample is recorded through a vacuum 3 m flight-path box to avoid parasitic scattering of the transmitted neutrons, covered with a large multi-bank  $^3\text{He}$ -filled tube detector up to  $120^\circ$  scattering angle. The incoming neutron wavelength is selected around  $\lambda = 1.1 \text{ \AA}$ , corresponding to a kinetic energy  $E_i = 67.6 \text{ meV}$ .

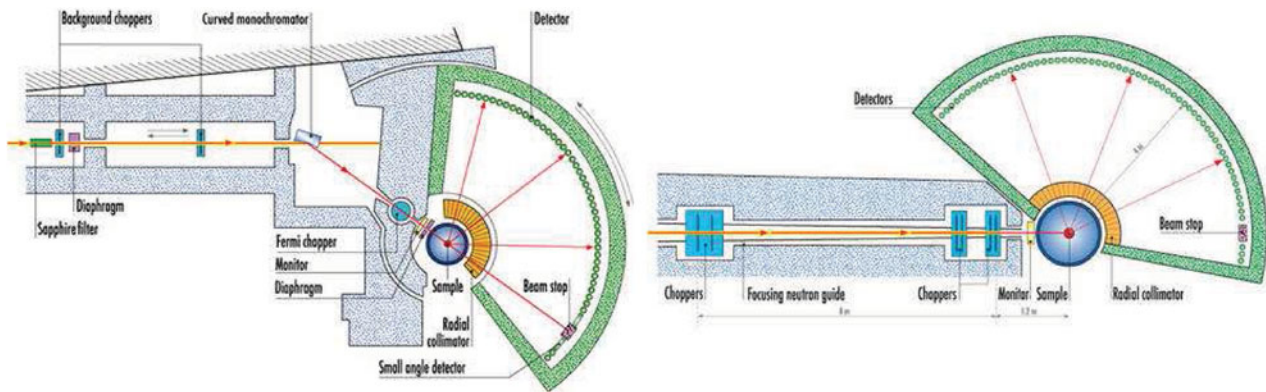


Figure 1. Schematic representation of the IN4 (left) and IN5 (right) time-of-flight neutron scattering spectrometers at the ILL, France, used to measure the dynamic structure factor of water.

The energy resolution on the elastic line  $\omega = 0$  is determined in this configuration from a measurement on a Vanadium incoherent scatterer reference sample as  $\delta\omega = 1.57$  meV (half-width). The accessible dynamic range measured with this instrument expands up to the energy transfer  $\omega = 100$  meV and the momentum transfer  $q = 10 \text{ \AA}^{-1}$ . Additional measurements with  $\lambda = 2.2 \text{ \AA}$  incident neutron wavelength have been acquired ( $E_i = 16.9$  meV,  $\delta\omega = 0.28$  meV half-width).

The IN5 instrument is a direct geometry multi-chopper neutron time-of-flight spectrometer used to study low-energy transfer processes as a function of momentum transfer [15]. The incident cold neutron beam from a high-intensity guide is pulsed and monochromatised through three counter rotating chopper pairs. An oscillating radial collimator is used to remove the contribution from the sample environment, while the scattered intensity from the sample is recorded on a  $30 \text{ m}^2$  cylindrical  $^3\text{He}$ -filled position sensitive detector mounted 4 m away from the sample inside a vacuum time-of-flight chamber. The instrument was used with an incident neutron wavelength  $\lambda = 2, 5$  and  $10 \text{ \AA}$ . The energy resolution achieved for  $\lambda = 2 \text{ \AA}$ , i.e.  $E_i = 20$  meV incident energy configuration is  $\delta\omega = 0.26$  meV (half-width), and the accessible dynamic range in this configuration extends up to the energy transfer  $\omega = 160$  meV and the momentum transfer  $q = 5.6 \text{ \AA}^{-1}$ . The IN5 instrument benefits from an excellent signal-to-noise ratio.

The micropore high-purity water samples were inserted in an aluminium flat container with thickness 0.05 and 0.25 mm for light and heavy water, respectively, with an indium wire sealing. Such high-precision containers are available at the ILL on time-of-flight spectrometers. The container was tilted by  $45^\circ$  to minimise self-shielding effects on the detector image. The sample was inserted inside a cryo-furnace allowing measurements from  $T = 10 \text{ K}$  up to  $350 \text{ K}$ . The light water sample scattering was measured at  $T = 285, 290, 294, 301, 311$  and  $323 \text{ K}$ . The heavy water sample scattering was measured at  $T = 295$  and  $325 \text{ K}$ .

The time-of-flight spectra measured at various angles are further treated in order to obtain the scattering function  $S(q, \omega)$  that is characteristic of the properties of the sample. The LAMP software [16] was used to read the IN4 and IN5 data-sets for the vanadium reference, the empty and the water filled sample cell. The data were normalised to the counting time, calibrated on the vanadium reference response, corrected for the detector energy-dependent efficiency, as well as for the sample flat cell tilted geometry, and finally converted from the radial angle and time space into the momentum and energy space representation to obtain the dynamic structure factor  $S(q, \omega)$ .

No multiple scattering correction was necessary, as the selected sample cell thickness 0.05 and 0.25 mm is much smaller than the neutron mean free path in water, estimated as 1.7 and 17.2 mm for light and heavy water, respectively, with a neutron incident wavelength  $\lambda = 2 \text{ \AA}$ . In order to check this assumption, we have simulated the spectrometer configuration with the templateTOF example instrument of the McStas package [17,18]. The sample was modelled with the Isotropic Sqw component [19] in a flat,  $45^\circ$  tilted geometry surrounded with an aluminium container. The simulation provides both the total scattering signal recorded on the spectrometer cylindrical detector, as well as the multiple scattering contribution. With the chosen cell thickness and experimental configuration, the multiple scattering contribution is then found smaller than 1% of the total scattering contribution, both for light and heavy water.

In the temperature range that was scanned during the measurement, the dynamic structure factor was found not to vary more than by a few per cent, so that we merged all acquisitions in order to improve the statistical accuracy. This approximation is in agreement with the previously measured variation of the structure factor with temperature, which does not exceed 3% between 275 and 348 K [20]. The effective temperature is then  $T = 307 \pm 14 \text{ K}$  and  $T = 310 \pm 17 \text{ K}$  for light and heavy water, respectively.

The symmetrised dynamic structure factor  $S^{\text{sym}}(q, \omega)$  is obtained from the dynamic structure factor  $S(q, \omega)$  by computing:

$$S(q, \omega) = \frac{\hbar\omega/k_B T}{1 - \exp(-\hbar\omega/k_B T)} S^{\text{sym}}(q, \omega), \quad (2)$$

which is simplified as  $S(q, \omega) \xrightarrow{\hbar\omega \ll k_B T} \exp(\hbar\omega/2k_B T) S^{\text{sym}}(q, \omega)$  in the so-called classical limit when the energy of the considered excitations in the liquid is smaller than the temperature. Our measurements extend to more than 100 meV in energy transfer, which is substantially larger than the equilibrium temperature energy  $k_B T = 25$  meV around  $T = 300$  K. Then, the classical limit does not hold at large energy transfer values. The ENDF documentation [21] reports computational accuracy issues for large energy transfer values, where the classical limit symmetrisation procedure does not hold, and may result in potentially unstable results. We thus make use of the afforded-mentioned extended symmetrisation relation which also holds at larger energy values.

The dynamic structure factor  $S(q, \omega)$  satisfies the detailed balance principle  $S(q, -\omega) = \exp(-\hbar\omega/k_B T) S(q, \omega)$  [13], whereas the symmetric counterpart satisfies  $S^{\text{sym}}(q, -\omega) = S^{\text{sym}}(q, \omega)$ .

The two separate measurements, performed using the IN4 and IN5 spectrometers, were combined using iFit [22] to obtain an effective scattering function on the widest possible dynamic range. The merging operation consists in computing the two IN4 and IN5 experimental data-sets on a common energy and wave-vector grid by means of a spline interpolant, then take the mean value of data-sets where they coexist on the grid, weighted by their respective measurement time, and actually taking into account the associated Jacobian of the transformation, so that the actual physical information is not affected (e.g. structure factors, DOS, etc.). This experimental symmetrised scattering function  $S^{\text{sym}}(q, \omega)$  for light and heavy water is shown in the **Figure 2**. Its actual energy resolution is estimated as 0.25 meV. The data-sets are limited by the measurable dynamical range, which is determined from the incident neutron energy and the detector geometry of the spectrometers. As expected, the light water dynamic structure factor exhibits a mostly incoherent scattering shape, whereas the heavy water one shows more pronounced coherent features at low momentum transfer. An excess scattering intensity shoulder can be seen around 80 and 50 meV energy transfer in light and heavy water, respectively, corresponding to the intra-molecular libration band.

## 2.2. Molecular dynamics simulations

In order to extend the measured dynamic range, we performed MD simulations. Two systems were prepared to perform the MD simulations. The first one consisted

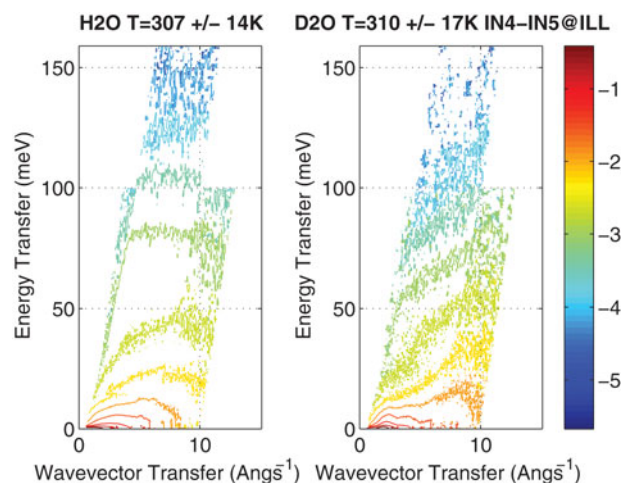


Figure 2. Symmetrised dynamic structure factor  $S^{\text{sym}}(q, \omega)$  of light (left) and heavy (right) water around 308 K, measured on the IN4 and IN5 neutron scattering spectrometers at the ILL. The  $S(q, \omega)$  contour plot is shown in  $\log_{10}$  scale.

in a  $50 \text{ \AA}^3$  box of 3921 TIP3P light water molecules [23] while in the second one, the mass of the hydrogen was replaced by the mass of deuterium in order to get a first approximation of heavy water. MD simulations were carried out with both systems using the following protocol.

- (1) Minimisation using the conjugate-gradient method (10,000 steps).
- (2) Heating of the system from 0 to 293 K by step of 20 K. For each temperature step, a 10 ps MD simulation was performed using NVT ensemble. The Langevin dynamics method was used for the thermostat.
- (3) Equilibration of the system at 293 K using a 10 ns MD simulation with NPT ensemble to keep the temperature at 293 K and the pressure at 1 bar. The Langevin dynamics method was used for the thermostat and the Langevin piston Nose-Hoover method was used for the barostat [24,25].
- (4) Production run at 293 K using 10 ps MD simulation with NVE ensemble. The MD frames were saved every 4 fs in order to get data sampled at high frequencies that could be used for a comparison on a large energy scale.

All the MD simulations were performed using periodic boundary conditions with a time step of 1 fs and all the covalent bonds treated as flexible. The simulations were performed using NAMD 2.7 program [26] with CHARMM 27 force field [27]. The TIP3P potential is not suitable to study the full water phase diagram [28], but it is known to model satisfactorily water molecule structure and dynamics around  $25^\circ \text{C}$  and 1 atm [23]. The potential equilibrium molecule configuration corresponds with an H-O-H angle of  $104.52^\circ$  and an O-H

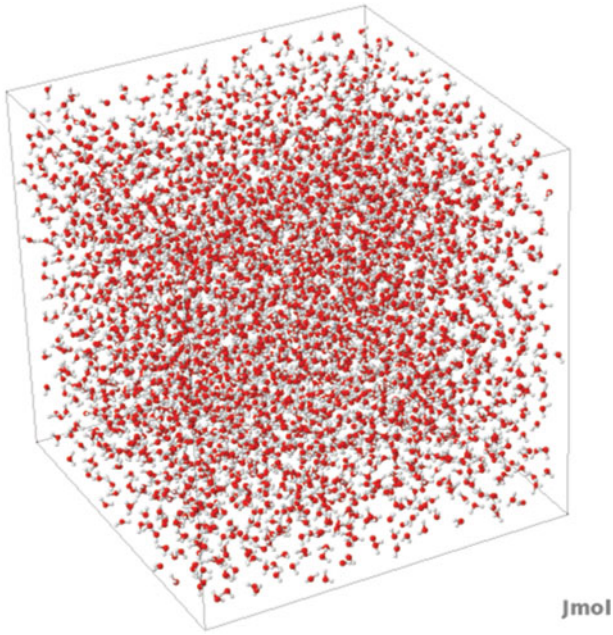


Figure 3. A snapshot of the MD simulation box, using the CHARMM TIP3P potential, showing the 3921 water molecules with Jmol.

distance of  $0.957 \text{ \AA}$ . The TIP3P potential was made flexible by relaxing the rigid bond constraint in the NAMD configuration file, so that intra-molecular modes can be accessed. The simulations were carefully checked, especially the NVE production run that actually showed a stable temperature around  $290 \pm 2 \text{ K}$ . This confirmed that the whole protocol led to an equilibrated system that could be sampled properly for a production run. A typical simulation box is shown in **Figure 3**.

The mean square displacement was computed from the trajectory, as shown in the **Figure 4**, using nMoldyn

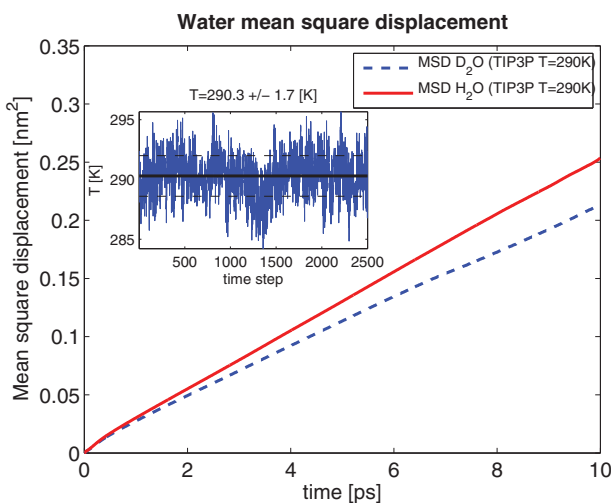


Figure 4. The mean square displacement of molecules extracted from the NAMD TIP3P MD simulation. The insert shows the system temperature along the trajectory.

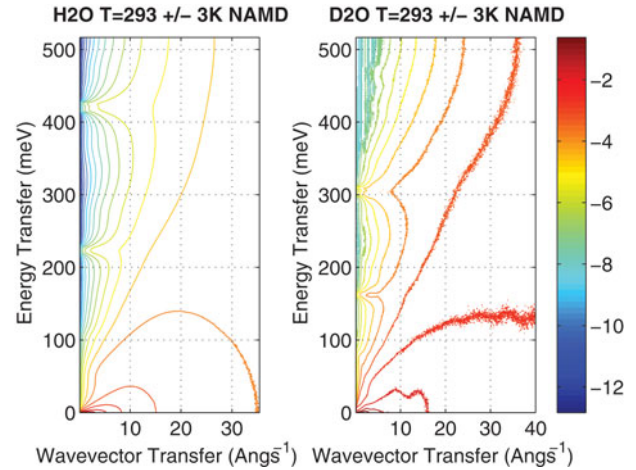


Figure 5. Symmetrised dynamic structure factor  $S^{\text{sym}}(q, \omega)$  of light (left) and heavy (right) water around 293 K, simulated using NAMD with a TIP3P potential. The  $S(q, \omega)$  contour plot is shown in  $\log_{10}$  scale.

[29,30]. The corresponding simulated diffusion coefficient at 290 K was found as  $4.1 \times 10^{-5}$  and  $3.5 \times 10^{-5} \text{ cm}^2/\text{s}$  for light and heavy water, respectively, slightly higher than the reported experimental value as  $2.3 \times 10^{-5} \text{ cm}^2/\text{s}$  in light water at 298 K [31]. The simulated diffusion coefficient is known to be highly dependent on the temperature and the potential model used [23,32]. Even though not perfect, we estimate that the TIP3P potential available in NAMD has sufficient accuracy to model light and heavy water systems in normal conditions for this study.

The dynamic structure factor was obtained from the trajectories by space and time Fourier transforms, using the nMOLDYN/MMTK software [29,30]. The momentum and energy smoothing filters used in the fast correlation algorithm were set to  $0.05 \text{ \AA}^{-1}$  and  $0.1 \text{ meV}$ , respectively. These quantities define an effective resolution assigned to the simulated dynamic structure factor. This procedure provides independently the coherent  $S_{\text{coh}}^{\text{sym}}$  and incoherent  $S_{\text{inc}}^{\text{sym}}$  contributions of the symmetrised dynamic structure factor.

In order to compare with our measurements of the total scattering dynamic structure factor, we then compute an effective simulated total scattering function as  $S^{\text{sym}} = (\sigma_{\text{coh}} S_{\text{coh}}^{\text{sym}} + \sigma_{\text{inc}} S_{\text{inc}}^{\text{sym}}) / (\sigma_{\text{coh}} + \sigma_{\text{inc}})$ , where  $\sigma_{\text{coh}}$  and  $\sigma_{\text{inc}}$  are the coherent and incoherent bound atom scattering cross-sections, respectively.

The resulting dynamic structure factor extends up to the energy transfer  $\omega = 500 \text{ meV}$  and the momentum transfer  $q = 40 \text{ \AA}^{-1}$ , as shown in **Figure 5**.

### 2.3. Discussion: structure and dynamics of water

The experimental structure factor  $S(q) = \int_{-\infty}^{\infty} S(q, \omega) d\omega$  inferred from this data-set for light and heavy water is shown in **Figure 6**. Previous experimental results are also reported [20,33].

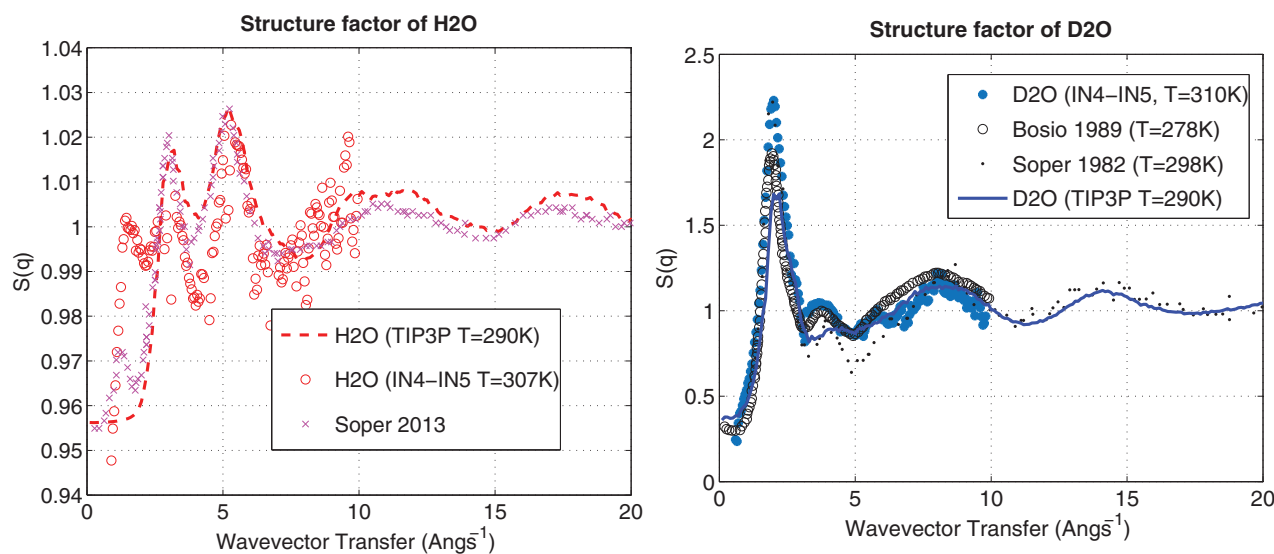


Figure 6. Structure factor of light (left) and heavy (right) water, measured on the IN4 and IN5 neutron scattering spectrometers at the ILL, compared with our MD simulation, and previous data [20,33]. The simulated data (TIP3P) is the sum of the coherent and incoherent structure factors weighted by the corresponding cross-sections.

The static structure factor can also be computed from the MD simulations, converting the simulated classical  $S^{\text{sym}}$  into  $S$  by applying Equation (2). The measured scattering structure factor is the sum of the coherent and incoherent scattering contributions. Consequently, the simulated data-set from MD has been computed as the sum of the coherent and incoherent structure factors weighted by the corresponding bound atom cross-sections. The general trend of the structure factor in our experimental data corresponds with that already reported [20,34] within 5%, even though with lower accuracy and local deviations. We conclude that the structure of water determined from experiments is well reproduced by our MD simulation, both for light and heavy water.

The vibrational frequency spectrum (density of states,  $\nu\text{DOS}$ )  $g(\omega)$  was extracted from the MD results, as the Fourier transform of the velocity auto-correlation function [30]. This quantity can be compared with the measured generalised density of states ( $g\text{DOS}$ ), which is related to the classical dynamic structure factor by [35]:

$$\lim_{q \rightarrow 0} \frac{\omega^2}{q^2} S_{\text{inc}}^{\text{sym}}(q, \omega) \simeq g(\omega). \quad (3)$$

As the incoherent (self) contribution is predominant in the light water scattering, due to its high incoherent scattering cross-section, the estimate of the  $g\text{DOS}$  from the total scattering experimental result is representative of the true DOS. However, in the case of heavy water including a substantial contribution from the coherent scattering, the estimate can only be approximate. This is indeed the case, as shown in Figure 7.

The simulated translational motions peak is found at 5.6 and 4.7 meV in light and heavy water, respectively. The corresponding peak in our experimental results is found at 6.7 and 7 meV, respectively. The simu-

lated water librational band is found at 55 and 37 meV in light and heavy water, respectively, whereas our experimental results indicate slightly higher energies. Previous results of the measured DOS in light water are also reported [36], in good agreement with this study. In light water, the simulated intra-molecular vibrational lines from the MD are found at 222 (bending), 416 and 425 meV (stretching). In heavy water, the same lines are found at 161 (bending), 299 and 308 meV (stretching). These values are slightly above the Fourier transform infrared spectroscopy (FT-IR) frequencies reported by Lappi [37], but below the coarse resolution density of state bands measured by Toukan [38]. From these results, we conclude that the MD simulation provides a realistic estimate of the water dynamics.

Finally, the water MD simulation and the measured scattering functions were combined using iFit [22], using the merge procedure detailed above, and are shown in the Figure 8. The experimental data-set has a lower statistical accuracy than the one provided by the MD, as seen from the dispersion of the contour lines in Figure 8, but they overlay satisfactorily. The final dynamic structure factor contains coherent and incoherent scattering contributions, both with elastic and inelastic processes.

This agreement between the experimental and the simulated dynamical structure factors allows to make use of the combined data-set as input to compute the total scattering cross-section, as well as the generation of ENDF and ACE format files for MCNP.

### 3. Total cross-sections for water

#### 3.1. Experimental cross-sections

The thermal neutron scattering cross-sections are used in the nuclear databases in their unit-less

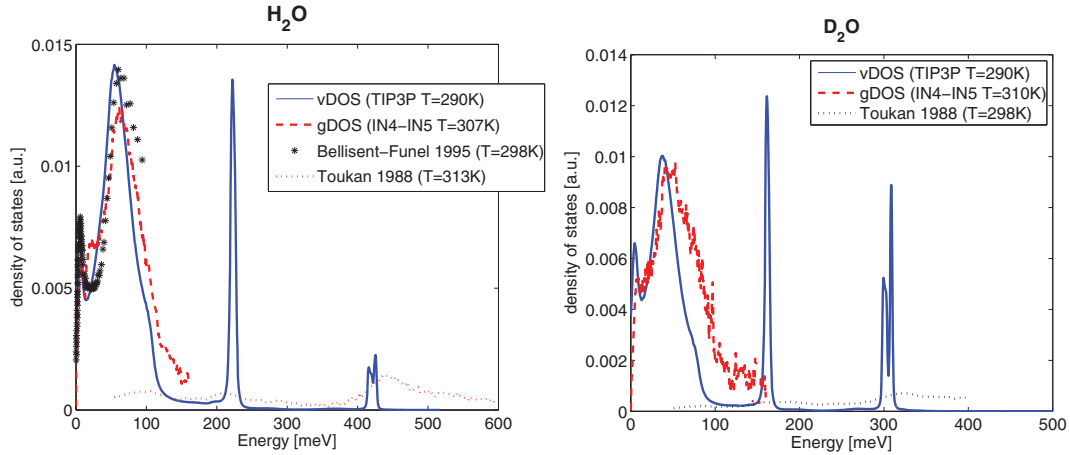


Figure 7. Vibrational DOS for light (left) and heavy (right) water as obtained from the MD velocity auto-correlation function (continuous line, vDOS) and from the neutron scattering experiment (approximate generalised density of states, gDOS). The experimental gDOS estimate for heavy water contains the coherent part, and is thus not exact. Data-sets were re-normalised so that the libration bands are similar. Previous data from Refs [36,38] are also reported.

representation, which corresponds to a variable change applied to the dynamic structure factor  $S(q, \omega)$ .

The scattering function  $S(q, \omega)$  can be transformed into the usual  $S(\alpha, \beta)$  law by:

$$S(\alpha, \beta) = k_B T \exp\left(\frac{-\hbar\omega}{2k_B T}\right) S(q, \omega) \simeq k_B T S^{\text{sym}}(q, \omega), \quad (4)$$

with the parameters:

$$\alpha = \frac{q^2 \hbar^2}{2Mk_B T} = \frac{E_i + E_f - 2\mu\sqrt{E_i E_f}}{Ak_B T}, \quad (5)$$

$$\beta = \frac{-\hbar\omega}{k_B T} = \frac{E_f - E_i}{k_B T}, \quad (6)$$

where  $\mu$  is the cosine of the scattering angle in the lab,  $m$  is the neutron mass,  $M$  is the water molecule mass and  $A = \frac{M}{m}$ . The function  $S(\alpha, \beta)$  is here used in its  $\beta$ -symmetric form, i.e.  $S(\alpha, \beta) = S(\alpha, -\beta)$ . In this expression,  $S(q, \omega)$  is the dynamic structure factor, which is related to its symmetric counterpart  $S^{\text{sym}}$  using Equation (2), shown in Figure 8.

As can be seen,  $S(\alpha, \beta)$  scales explicitly on the temperature  $T$ , as well as the  $(\alpha, \beta)$  inverse values, whereas  $S^{\text{sym}}(q, \omega)$  often changes only close to phase transitions. This means that, assuming the material is not considered close to a transition, a single  $S^{\text{sym}}(q, \omega)$  data-set at a given temperature  $T$  may be used to derive the  $S(\alpha, \beta)$  values in a temperature range around  $T$ . As stated previously, the temperature effect on the water structure factor is limited to 1–3 per cent in the measurement temperature range, i.e. 285–325 K. We may then derive, from a single dynamic structure factor  $S^{\text{sym}}(q, \omega)$  around 300 K, a full set of  $S(\alpha, \beta)$  in the range 285–325 K.

The double differential thermal neutron scattering cross-section is then given by:

$$\frac{d^2\sigma}{d\Omega dE_f}(E_i, E_f, \Omega) = \frac{\sigma_b}{4\pi k_B T} \sqrt{\frac{E_f}{E_i}} e^{-\beta/2} S(\alpha, \beta), \quad (7)$$

which is equivalent to Equation (1).

The total thermal neutron scattering cross-section is obtained by integrating Equation (7), first on  $\mu$  from  $-1$  to  $1$  and then on  $E_f$  from  $0$  to  $+\infty$ . Performing the variable substitution  $(\mu, E_f) \rightarrow (\alpha, \beta)$ , the thermal neutron scattering cross-section at the temperature  $T$  becomes:

$$\sigma_T(E) = A k_B T \frac{\sigma_b}{4E} \int_{-E_i/(k_B T)}^{+\infty} \int_{\alpha_{\min}}^{\alpha_{\max}} S(\alpha, \beta) e^{-\beta/2} d\alpha d\beta, \quad (8)$$

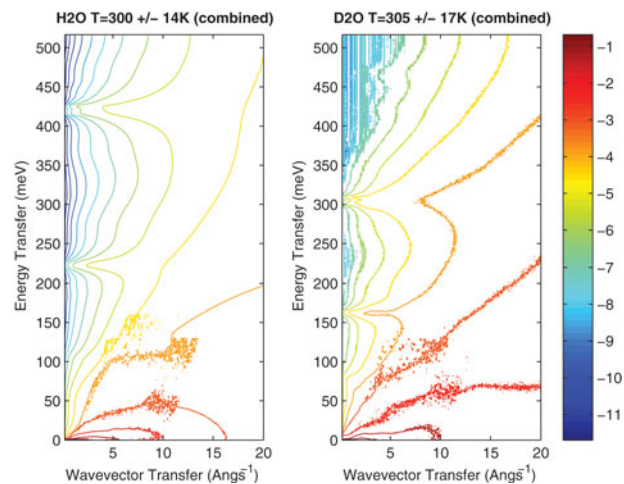


Figure 8. Symmetrised dynamic structure factor  $S^{\text{sym}}(q, \omega)$  of light (left) and heavy (right) water around 300 K, combining MD and experimental data-sets. The  $S(q, \omega)$  contour plot is shown in  $\log_{10}$  scale.

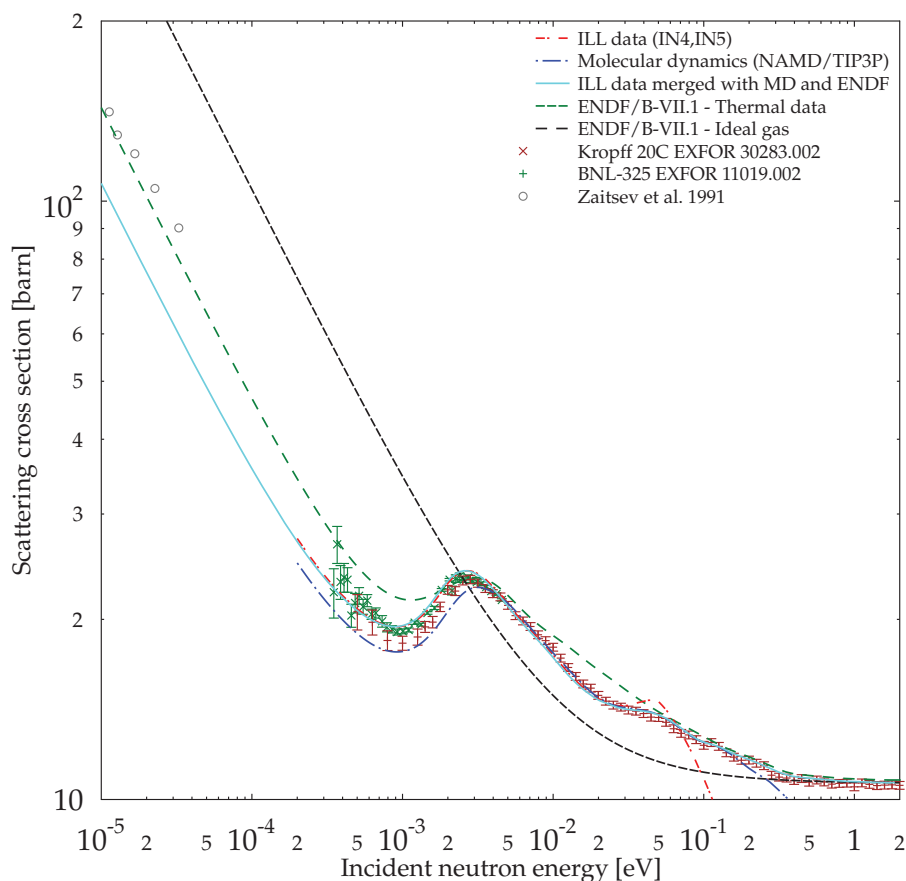


Figure 9. Neutron scattering cross-section of heavy water at 300 K, per  $D_2O$  molecule. Our results are indicated as dash-dotted and continuous lines. Previous experimental data (crosses) are obtained from [39,40].

with

$$\alpha_{\min} = \frac{(\sqrt{E_i} - \sqrt{E_f})^2}{Ak_B T} \quad \text{and} \quad \alpha_{\max} = \frac{(\sqrt{E_i} + \sqrt{E_f})^2}{Ak_B T}. \quad (9)$$

This scattering cross-section behaves asymptotically as  $k_B T/E$  in the thermal energy range.

The scattering cross-section corresponding to our experimental  $S(\alpha, \beta)$  is plotted in red in Figure 9 for heavy water, for neutron energies ranging from 0.2 to 100 meV. The same figure shows the cross-section obtained using the  $S(\alpha, \beta)$  from ENDF/B.VII.1 library (green curve) and the cross-section corresponding to the ideal gas approximation (black curve). Experimental values obtained from previous total cross-section measurements are also depicted: the brown and green crosses were found in the EXFOR database [39], the first corresponds to EXFOR number 11019002 and the second to EXFOR number 30283002. The grey circles were found in Ref. [40].

The shape of the neutron scattering cross-section calculated from our experimental  $S(\alpha, \beta)$  appears to be in agreement with previous data up to 24 meV inci-

dent neutron energy. Especially, it behaves better than ENDF/B.VII.1 between 0.5 and 24 meV. The peak around 3 meV incident neutron energy originates from the fact that the integration range in Equation (8) then fully includes the heavy water structure peak, bringing an additional scattering probability on the water molecule first diffraction sharp peak (see Figure 6). In light water, the structure factor is mostly incoherent and does not exhibit any marked diffraction peak. No such local maximum can be seen in the total scattering cross-section (see Figure 10), which is much smoother.

Above that range, from 24 to 50 meV, our heavy water thermal scattering cross-section estimate shows an excess which may be due to the experimental noise on highest neutron energy transfer measurements (100–160 meV). This noise, which actually reaches the instrument background level as seen in Figure 2, and is more pronounced in the experiments using IN4, is amplified by the  $e^{-\beta/2}$  factor in Equation (8). Above 50 meV incident neutron energy, the cross-section decreases quickly as the integration domain in Equation (8) becomes larger than the domain where  $S(\alpha, \beta)$  has been measured. Indeed, the measurement range goes from  $\beta = -\beta_{\max}^{EXP}$  to

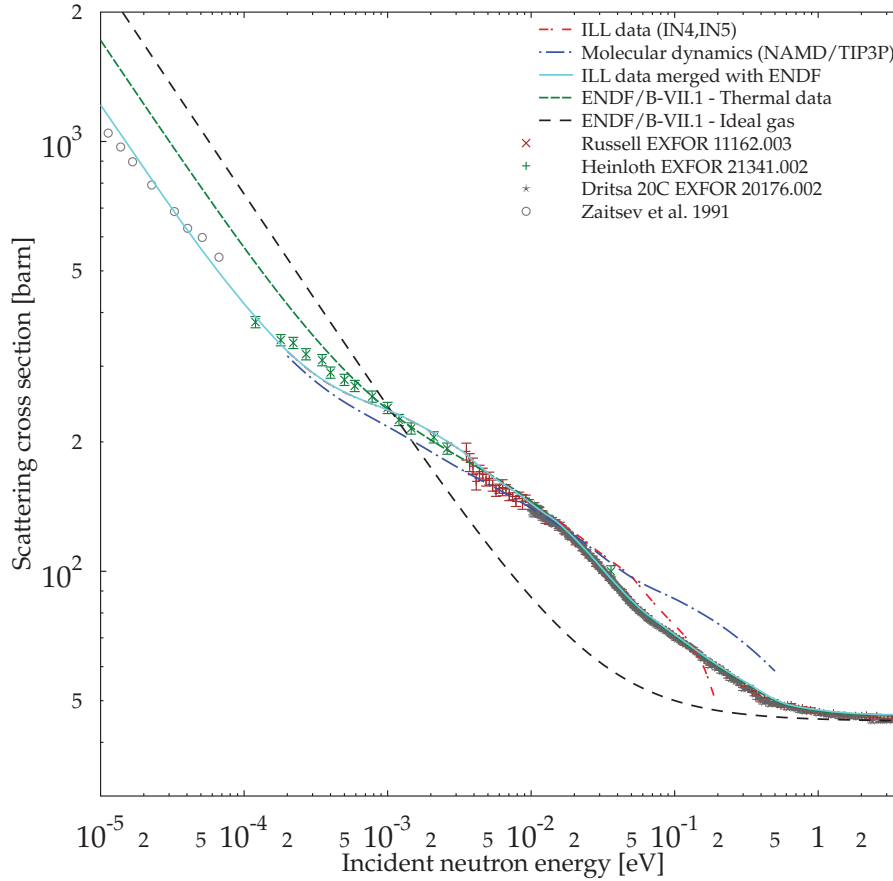


Figure 10. Neutron scattering cross-section of light water at 300 K, per  $\text{H}_2\text{O}$  molecule. Our results are indicated as dash-dotted and continuous lines. Previous experimental data (crosses, circle) are obtained from [39,40].

$\beta_{\max}^{EXP} = 5.989$ , and from  $\alpha = 0$  to  $\alpha_{\max}^{EXP} = 0.8843$ . The scattering cross-section can then be obtained with Equation (8) only for energies  $E_i$  such as:

$$\frac{-E_i}{kT} \geq -\beta_{\max}^{EXP} \quad \text{and} \quad \frac{(\sqrt{E_i} + \sqrt{E_f})^2}{Ak_B T} \leq \alpha_{\max}^{EXP}. \quad (10)$$

Considering the maximum measured energy transfer, 100 meV on IN4 and 160 meV on IN5 (see Figure 2), we find that the limits of the integral Equation (8) exceed the measured dynamic range for an incident energy above 24 meV. This value simply matches the effective incident neutron energy implied when merging the IN4 and IN5 spectrometer experiments at  $\lambda \simeq 2 \text{ \AA}$ , i.e.  $E_i \simeq 20 \text{ meV}$ .

Considering this limitation, it is advisable to extend experimental  $S(\alpha, \beta)$  in order to obtain the scattering cross-section on a larger thermal energy domain, as discussed below.

For light water, the same treatment was performed. Figure 10 depicts the corresponding scattering cross-sections with the same colours as in the heavy water case, for neutron energies ranging from 0.2 to 200 meV. Here the measured cross-section values were found in Ref. [40] (grey circle) and in EXFOR database: brown

crosses correspond to EXFOR number 11162003, green crosses to EXFOR number 21341002 and grey crosses to EXFOR number 20176002. The cross-section calculated from our experimental  $S(\alpha, \beta)$  follows quite well the measured values until about 15 meV, but similarly as for heavy water it then exhibits an excess intensity before actually decreasing because of the experimental domain limitations.

Light water is nearly a pure incoherent scatterer, with an intense quasi-elastic scattering signal at low  $q$  value. At these momentum values, the experimental data-set, as seen in Figure 2, is limited to a maximum energy transfer of 100 meV (from the IN4 experiment), but this sharp contribution constitutes a major part of the scattering cross-section Equation (8). When taking into account this restriction, we find out that the integration range does not allow to compute accurately the cross section above 16 meV, which corresponds to the IN4 configuration using the incident neutron wavelength  $\lambda = 2.2 \text{ \AA}$ .

### 3.2. Cross sections from combined experiments and molecular dynamics

The scattering cross section can be computed from Equation (8) when using the dynamic structure factor

obtained from the MD simulation in Figure 5. In this case, the available dynamic range  $(\alpha, \beta)$  is much larger than that covered by the experiments.

For heavy water, the cross section calculated from the  $S^{\text{MD}}(\alpha, \beta)$  obtained by MD simulations is plotted in blue in Figure 9.

We compute the combined  $S(\alpha, \beta)$  so that the corresponding cross section is equal to the cross section calculated from  $S^{\text{EXP}}(\alpha, \beta)$  until an incident neutron energy  $E_c = 24$  meV and becomes equal to the cross section calculated from  $S^{\text{MD}}(\alpha, \beta)$  after  $E_c$ . These new  $S(\alpha, \beta)$  values are obtained on the union of the  $(\alpha, \beta)$  grids from our MD simulations and experiments. When a point  $(\alpha, \beta)$  of the new grid is inside the definition domain of  $S^{\text{EXP}}(\alpha, \beta)$  and inside the integration domain needed to calculate the cross section at 24 meV (which roughly coincide and are given by the mean incident neutron energy used during the experiments), i.e.  $\beta \geq -E_c/(kT)$  and  $\frac{(\sqrt{E_c - \sqrt{E_c + \beta kT}})^2}{AkT} \leq \alpha \leq \frac{(\sqrt{E_c + \sqrt{E_c + \beta kT}})^2}{AkT}$ , then we take  $S(\alpha, \beta) = S^{\text{EXP}}(\alpha, \beta)$ . In all the other cases, we take  $S(\alpha, \beta) = S^{\text{MD}}(\alpha, \beta)$ . This method guaranties that the cross section calculated from the new  $S(\alpha, \beta)$  is continuous at  $E = E_c$  when switching from the experimental data only, to the data-set extended with the MD scattering function.

In Figure 9, we notice that the cross-section calculated from  $S^{\text{MD}}(\alpha, \beta)$  is close to the measured values until an incident neutron energy of 160 meV. Yet, the cross-section from ENDF/B.VII.1  $S(\alpha, \beta)$  is close to the measured values above 160 meV. Besides, at this energy, the computed cross-sections from  $S^{\text{MD}}(\alpha, \beta)$  and from ENDF/B.VII.1 are roughly equal. Thus, as our objective is still to produce a  $S(\alpha, \beta)$  allowing to reproduce experimental cross-section values, we replace the  $S(\alpha, \beta)$  value used in the integration domain needed for the cross-section computation above an incident energy of 160 meV calculations by the value of the  $S(\alpha, \beta)$  from ENDF/B.VII.1. The final  $S(\alpha, \beta)$  is an overlay of our  $S^{\text{EXP}}(\alpha, \beta)$  (until an incident neutron energy of 24 meV), of  $S^{\text{MD}}(\alpha, \beta)$  (from 24 to 160 meV incident neutron energy) and of the ENDF/B.VII.1  $S(\alpha, \beta)$  (above 160 meV incident neutron energy). The corresponding cross-section is plotted in cyan in Figure 9. We can verify that it follows quite well the experimental cross-section values at all energies.

For light water, the cross-section obtained from  $S^{\text{MD}}(\alpha, \beta)$  is plotted in blue in Figure 10. The cross-section calculated with  $S^{\text{EXP}}(\alpha, \beta)$  is acceptable until 15 meV (in red). But, above this energy, the MD simulation does not substantially improve the behaviour of the cross-section. On the other hand, the cross-section from ENDF/B.VII.1 describes well the previous measurements of the total scattering above an incident neutron energy of 15 meV. Therefore, we choose our new function  $S(\alpha, \beta)$  by taking  $S^{\text{EXP}}(\alpha, \beta)$  until 15 meV incident neutron energy and  $S(\alpha, \beta)$  from ENDF/B.VII.1 above 15 meV incident neutron energy. Figure 10

depicts the corresponding combined cross-section in cyan.

The fact that the ENDF/B.VII.1 original data-set accurately describes the light water cross-section is not surprising. Indeed, light water is mostly an incoherent scatterer. Moreover, light water does not exhibit strong coherent features, such as structural peaks and phonons. In this respect, all scattering processes considered in LEAPR [1] are well suited to describe light water.

We would like to stress here that our new scattering functions  $S(\alpha, \beta)$  data-sets, and the inferred thermal neutron scattering cross-sections, only depend on the legacy analytical models above 160 meV incident energy in heavy water, and 15 meV in light water. Below these values, the full structural and dynamical information has been taken into account. The new  $S(q, \omega)$  dynamic structure factor files for light and heavy water will be distributed with the McStas [17, 18] software, and are available as Supplemental data.

### 3.3. Neutron scattering data in the ENDF and ACE format

Having determined the scattering law  $S(\alpha, \beta)$  on a large domain for light and heavy water, we can produce an input file for MCNP calculations, in the ACE format. We make use of the THERMR and ACER modules of NJOY [1]. THERMR can read the  $S(\alpha, \beta)$  in an ENDF file [21] and process the corresponding cross-section and differential cross-section. ACER can then use THERMR output to produce an ACE file. Our first step is then to produce the input ENDF file for THERMR.

The  $S(\alpha, \beta)$  scattering function as shown in Figure 8 corresponds to a whole water molecule, but the ENDF format requires to provide data for a single atom H or D. In the heavy water case, we label with a subset D the quantities corresponding to a deuterium atom, with the subset O the ones corresponding to an oxygen atom, and without subsets the ones corresponding to the whole water molecule. The ENDF manual [21] computes the thermal neutron double differential scattering cross-section of the molecule as the sum of separate contributions per atom, ignoring e.g. the cross oxygen–deuterium term:

$$\frac{d^2\sigma_T}{d\Omega dE_f}(E_i, E_f, \Omega) = \frac{1}{4\pi k_B T} \sqrt{\frac{E_f}{E_i}} e^{-\beta/2} \times [2\sigma_{b,D} S_D(\alpha_D, \beta) + \sigma_{b,O} S_O(\alpha_O, \beta)], \quad (11)$$

with

$$\alpha_D = \frac{E_i + E_f - 2\mu\sqrt{E_i E_f}}{A_D k_B T} \quad \text{and} \quad \alpha_O = \frac{E_i + E_f - 2\mu\sqrt{E_i E_f}}{A_O k_B T}, \quad (12)$$

where  $A_D$  and  $A_O$  are, respectively, the masses of deuterium and oxygen in neutron mass unit. With  $\sigma_b = 2\sigma_{b,D} + \sigma_{b,O}$ , the  $S(\alpha, \beta)$  for one deuterium atom is:

$$S_D(\alpha_D, \beta) = \frac{\sigma_b}{2\sigma_{b,D}} S(\alpha, \beta) - \frac{\sigma_{b,O}}{2\sigma_{b,D}} S_O(\alpha_O, \beta). \quad (13)$$

We currently only have access to the total scattering law of the light water molecule. As deuterium is the principal scatterer in the heavy water molecule (or hydrogen in the light water), we shall consider its contribution as a perturbation in the total molecule scattering, and approximate its scattering law  $S_O(\alpha_O, \beta)$  using available models in ENDF. We use the free gas law (as in Ref. [6]):

$$S_O(\alpha_O, \beta) = \frac{1}{\sqrt{4\pi\alpha_O}} \exp\left(-\frac{\alpha_O^2 + \beta^2}{4\alpha_O}\right). \quad (14)$$

The same treatment is applied to light water. As a check of the procedure, the scattering cross-section of water is calculated back, adding twice the one of hydrogen and once the one of oxygen according to Equation (13). This formalism, which ignores the oxygen–deuterium cross terms, is clearly inaccurate, but corresponds to the procedure used in ENDF to compute any material cross-section from its single atom contributions. In this study, the cross-term is implicitly included in the deuterium one. In the case of light water, the hydrogen contribution is much higher than the other oxygen and oxygen–hydrogen terms, and the approximation is fully justified. In heavy water, the deuterium scattering cross-section remains higher than the oxygen one, and the approximation may be retained, even though coarse. The total scattering cross-section is obtained by integration of Equation (8). The MD simulation can provide partial scattering laws, e.g. for oxygen in water, so that we may in the future make use of this information to extract a better estimate of the hydrogen and deuterium partial scattering laws, as well as cross-terms, in the energy domain handled by the MD.

Once the ENDF files for H in  $H_2O$ , and for D in  $D_2O$ , have been constructed, we can run the module THERMR of NJOY 99.259. The grid in  $\alpha$  and  $\beta$  needed to include the experimental and MD results requires a fine sampling, beyond the current NJOY memory handling capabilities. We have thus slightly modified NJOY to make it able to process our large  $S(\alpha, \beta)$  files. The use of ACER did not raise any particular issue. The new  $S(\alpha, \beta)$  ACE files for light and heavy water are available as Supplemental data.

#### 4. Benchmark of the Institut Laue-Langevin reactor

The processed  $S(\alpha, \beta)$  files have been tested on the MCNP IRPhEP benchmarked model of the ILL Réacteur à Haut Flux (RHF) [7]. The RHF is dedicated to thermal neutron production for scientific experiments. The reactor is cooled and moderated by heavy

Table 1. IRPhEP benchmark configurations of the RHF model. Values should be around 0 pcm.

Case	Configuration	$k_{\text{eff}}$	Uncertainty	$\frac{C-E}{E}$ (pcm)
1	All SR up	0.99817	0.00003	–
2	SR1 down	1.00232	0.00007	415
3	SR2 down	1.00036	0.00007	219
4	SR3 down	1.00055	0.00007	238
5	SR4 down	1.00283	0.00007	466
6	SR5 down	1.00125	0.00007	308
7	SR1 and SR2 down	1.00112	0.00007	295
8	SR1 and SR5 down	1.00143	0.00007	326

water. It has only one fuel element, based upon the Oak Ridge National Laboratory High Flux Isotope Reactor (HFIR) design. The RHF MCNP model is based upon a sub-critical approach with all five SR in different positions. It uses the ENDF/B-VII.0 library. Its overall error has been assessed to +234/–231 pcm at  $1\sigma$ . **Table 1** shows the benchmarked configurations. The reference one (case 1) is defined with the five SR are in the upper position, i.e. when the absorbing tube is far from the fuel element. Then, each SR is individually set in the down position (cases 2–8) in order to assess their anti-reactivity. The  $\frac{C-E}{E}$  ratio, where  $C$  is the calculated criticality factor  $k_{\text{eff}}$  and  $E$  the experimental one, in **Table 1** shows a large discrepancy when comparing case 1 to each of cases 2–8. The latter cases are always above the reference case 1 by hundreds of pcm, most of them being above  $1\sigma$  of the model uncertainty. Yet, it remains less than  $3\sigma$ ; this highlights clearly the model sensibility when any absorber is put within the reactor pool.

When the new  $S(\alpha, \beta)$  files are used for deuterium within heavy water, we get significant changes in the resulting  $k_{\text{eff}}$  and  $\frac{C-E}{E}$ , as indicated in **Table 2**. The difference between the model and the experimental  $k_{\text{eff}}$  is now statistically centred around zero, as expected.

Our experimental dynamic structure factor was found to vary by less than 3% between 285 and 325 K, i.e. 0.07%/K, in agreement with [20]. In addition, as the  $S(\alpha, \beta)$  law scales mostly linearly with temperature, the direct temperature variation is  $1/300 = 0.3\%/K$ . Consecutively, we may estimate the variation on  $S(\alpha, \beta)$  from Equation (4) to be at most 0.3–0.4%/K. The total scattering cross-section Equation (8) logically follows

Table 2. Benchmark configurations of the RHF model with the new  $S(\alpha, \beta)$  of deuterium in heavy water.

Case	Configuration	$k_{\text{eff}}$	Uncertainty	$\frac{C-E}{E}$ (pcm)
1	All SR up	1.00319	0.00007	–
2	SR1 down	1.00505	0.00007	30
3	SR2 down	1.00338	0.00007	–132
4	SR3 down	1.00343	0.00007	–129
5	SR4 down	1.00567	0.00007	109
6	SR5 down	1.00465	0.00007	–8
7	SR1 and SR2 down	1.00246	0.00007	–73
8	SR1 and SR5 down	1.00217	0.00007	–101

the same behaviour. However, in that range, the calculated temperature variation of the criticality factor  $k_{\text{eff}}$  for the full IRPhEP benchmark model is found to be only 10 pcm/K, that is 0.01%/K. We conclude that the criticality factor sensitivity on the temperature is 30–40 times smaller than that of the thermal neutron scattering cross-section for water. When propagating the uncertainty on the experimental data, that is 3%, the inferred uncertainty on  $k_{\text{eff}}$  is found to be at most 95 pcm, which is smaller than the improvement seen on the benchmark, and then the intrinsic model uncertainty of 231 pcm [7].

Thus, we can conclude that the use of our improved  $S(\alpha, \beta)$  cross-sections clearly leads to more accurate results for the RHF model. Obviously, this does not fully qualify our new  $S(\alpha, \beta)$  cross-sections. This only shows that they may bring a positive impact on the RHF model which is a relevant benchmark because of its pure heavy water pool. However, we believe that our new methodology, which allows to take into account the low-energy dynamics and the structure of water in the neutron cross-sections, can benefit to other neutron transport models and provide a better accuracy.

## 5. Conclusions

In this paper, we show a way to implement measured  $S(\alpha, \beta)$  into the ACE format. This is a very promising solution to improve the thermal neutron cross-section reliability. The gain in accuracy is mostly restricted to energies lower than 160 and 15 meV for heavy and light water, respectively. Extension to higher energy ranges could be envisaged with further experiments on the ILL hot neutrons instruments or on spallation sources like ISIS, SNS, where higher neutron energies are available. Also, the partial dynamic structure factors of atoms, obtained from MD, may be used to improve further the accuracy of the hydrogen and deuterium scattering cross-sections and differential cross-sections.

Furthermore, we are interested in recording the spectra of the most common materials in the nuclear field like water, lanthanide nitrate solutions, polyethylene, liquid deuterium, methane, beryllium, mesitylene, etc. We are also looking for reproducing the common industrial operating conditions, like those of the pressured water reactors (350 °C and 150 bar) for example.

## Acknowledgements

We gratefully thank S. Rols and J. Ollivier for their support on the IN4 and IN5 time-of-flight spectrometers at the ILL, as well as the whole ILL staff for their efficient work. The ILL scientific computing resources have been used for the data treatment and the MD simulations. M. Gonzalez and E. Guarini contributed to vivid discussions regarding the data analysis.

## Supplemental data

Supplemental data for this article can be accessed here.

## References

- [1] MacFarlane R, Muir D. The NJOY nuclear data processing system. Los Alamos: Los Alamos National Laboratory; 1994. (Report LA-12470-M).
- [2] Cullen D, Blomquist R, Dean C, Heinrichs D, Kalugin M, Lee M, Lee YK, MacFarlane R, Nagaya Y, Trkov A. How accurately can we calculate neutrons slowing down in water? Livermore (CA): Lawrence Livermore National Laboratory; 2006. (Report UCRL-TR-220605).
- [3] Cullen D, Blomquist R, Green M, Lent E, MacFarlane R, McKinley S, Plechaty E, Sublet JC. How accurately can we calculate neutrons slowing down in water? Livermore (CA): Lawrence Livermore National Laboratory; 2006. (Report UCRL-TR-220605).
- [4] Svenne JP, Canton L, Kozier K, Townsend L. Re-evaluating low-energy neutron-deuteron elastic scattering using three-nucleon theory. Paper presented at: International Conference on Nuclear Data for Science and Technology; 2007 April 22–27; Nice, France; p. 243–246. doi:10.1051/ndata:07208
- [5] van der Marck SC. Benchmarking ENDF/B-VII.0. Nuclear Data Sheets. 2006;107:3061–3118. doi:10.1016/j.nds.2006.11.002
- [6] Mattes M, Keinert J. Thermal neutron scattering data for the moderator materials  $H_2O$ ,  $D_2O$  and  $ZrH_x$  in ENDF-6 format and as ACE library for MCNP(X) codes. International Nuclear Data Committee; 2005. (Report INDC(NDS)-0470).
- [7] Calzavara Y. Evaluation of measurements performed on the French high flux reactor (HFR). Paper presented at: International Reactor Physics Benchmark Experiments Project; 2008 October 20–24; Paris, France. (Report OECD/NEA HFR-HWR-RESR-001CRIT).
- [8] Haeck W, Leclaire N. Thermal scattering data and criticality safety. Presented at: International Conference on the Physics of Reactors (PHYSOR); 2008 September 14–19; Interlaken, Switzerland.
- [9] Trkov A, Mattes M. On the thermal scattering law data for reactor lattice calculations. Paper presented at: Nuclear Energy for Europe 2004; 2004 September 6–9; Portoro, Slovenia.
- [10] Marquez Damian JI, Malaspina DC, Granada JR. Vibrational spectra of light and heavy water with application to neutron cross section calculations. J Chem Phys. 2013;139:024504. doi:10.1063/1.4812828
- [11] Marquez Damian JI, Granada JR, Malaspina DC. CAB models for water: a new evaluation of the thermal neutron scattering laws for light and heavy water in ENDF-6 format. Ann Nucl Energy. 2014;65:280–289. doi:10.1016/j.anucene.2013.11.014
- [12] Santamarina A, Bernard D, Blaise P, Coste M, Courcelle A, Huynh C, Jouanne TD, Leconte P, Litaize O, Mengelle S, Nogure G, Ruggieri J-M, Srot O, Tommasi J, Vaglio C, Vidal J-F. The JEFF-3.1.1 nuclear data library; 2009. (Report OECD/NEA No. 6807).
- [13] Squires GL. Thermal neutron scattering. Cambridge (UK): Cambridge University Press; 1978. ISBN 0521218845.
- [14] Mutka H. Coupled time and space focusing for time-of-flight inelastic scattering. Nucl Instruments Methods A. 1994;338:144–150. Available from: <http://www.ill.eu/in4c>. DOI: 10.1016/S0921-4526(99)01366-6
- [15] Ollivier J, Mutka H. IN5 cold neutron time-of-flight spectrometer, prepared to tackle single crystal spectroscopy. J Phys Soc Japan. 2011;80:SB003. doi:10.1143/jpsjs.80sb.sb003. Available from: <http://www.ill.eu/in5>

- [16] Richard D, Ferrand M, Kearley GJ. Analysis and visualisation of neutron-scattering data. *J Neut Res.* 1996;4:33–39. doi:10.1080/10238169608200065. Available from: [http://www.ill.fr/data\\_treat/lamp/lamp.html](http://www.ill.fr/data_treat/lamp/lamp.html)
- [17] Lefmann K, Nielsen K. McStas, a general software package for neutron ray-tracing simulations. *Neutron News.* 1999;10:20–23. doi:10.1080/10448639908233684. Available from: <http://www.mcstas.org>
- [18] Willendrup P, Farhi E, Lefmann K. McStas 1.7 – a new version of the flexible Monte Carlo neutron scattering package. *Physica B.* 2004;350:e735–e737. doi:10.1016/j.physb.2004.03.193
- [19] Farhi E, Hugouvieux V, Johnson MR, Kob W. Virtual experiments: combining realistic neutron scattering instrument and sample simulations. *J Comput Phys.* 2008;228:5251–5261. doi:10.1016/j.jcp.2009.04.006
- [20] Bosio L, Teixeira J, Bellissent-Funel M-C. Enhanced density fluctuations in water analyzed by neutron scattering. *Phys Rev A.* 1989;39:6612–6613. doi:10.1103/PhysRevA.39.6612
- [21] Herman M, Trkov A. ENDF-6 formats manual: data formats and procedures for the evaluated nuclear data files ENDF/B-VI and ENDF/B-VII. New York: Brookhaven National Laboratory; 2009. (CSEWG Document ENDF-102/Report BNL-90365-2009 Rev.1).
- [22] Farhi E, Debab Y, Willendrup P. iFit: a new data analysis framework. Applications for data reduction and optimization of neutron scattering instrument simulations with McStas. *J Neutron Res.* 2013;17:5–18. doi:10.3233/JNR-130001. Available from: <http://ifit.mccode.org>
- [23] Jorgensen WL, Chandrasekhar J, Madura JD, Impey RW, Klein ML. Comparison of simple potential functions for simulating liquid water. *J Chem Phys.* 1983;79:926–935. doi:10.1063/1.445869
- [24] Feller SE, Zhang Y, Pastor RW, Brooks BR. Constant pressure molecular dynamics simulation: the Langevin piston method. *J Chem Phys.* 1995;103(11):4613–4622. doi:10.1063/1.470648
- [25] Martyna GJ, Tobias DJ, Klein ML. Constant pressure molecular dynamics algorithms. *J Chem Phys.* 1994;101(5):4177–4189. doi:10.1063/1.467468
- [26] Phillips JC, Braun R, Wang W, Gumbart J, Tajkhorshid E, Villa E, Chipot C, Skeel RD, Kale L, Schulten K. Scalable molecular dynamics with NAMD. *J Comput Chem.* 2005;26:1781–1802. doi:10.1002/jcc.20289
- [27] MacKerell Jr, Banavali N, Foloppe N. Development and current status of the CHARMM force field for nucleic acids. *Biopolymers.* 2001;56(4):257–265. doi:10.1002/1097-0282(2000)56:4<257::AID-BIP10029>3.0.CO;2-W
- [28] Vega C, Abascal JLF, Sanz E, MacDowell LG, McBride C. Can simple models describe the phase diagram of water? *J Phys.* 2005;17:S3283–S3288. doi:10.1088/0953-8984/17/45/013
- [29] Hinsén K, Pellegrini E, Stachura S, Kneller GR. nMoldyn 3: using task farming for a parallel spectroscopy-oriented analysis of molecular dynamics simulations. *J Comput Chem.* 2012;33:2043–2048. doi:10.1002/jcc.23035
- [30] Rog T, Murzyn K, Hinsén K, Kneller GR. nMoldyn: a program package for a neutron scattering oriented analysis of molecular dynamics simulations. *J Comput Chem.* 2003;24:657–667. doi:10.1002/jcc.10243
- [31] Krynicki K, Green CD, Sawyer DW. Pressure and temperature dependence of self-diffusion in water. *Faraday Discuss Chem Soc.* 1978;66:199–208. doi:10.1039/DC9786600199
- [32] Mark P, Nilsson L. Structure and dynamics of the TIP3P, SPC, and SPC/E water models at 298 K. *Phys Chem A.* 2001;105:9954–9960. doi:10.1021/jp003020w
- [33] Soper AK, Silver HN. Hydrogen-hydrogen pair correlation function in liquid water. *Phys Rev Lett.* 1982;49:471–474. doi:10.1103/PhysRevLett.49.471
- [34] Soper AK. The radial distribution functions of water as derived from radiation total scattering experiments: is there anything we can say for sure? *ISRN Phys Chem.* 2013;2013:ID279463. doi:10.1155/2013/279463
- [35] Bellissent-Funel M-C, Teixeira J. Dynamics of water studied by coherent and incoherent inelastic neutron scattering. *J Mol Struct.* 1991;250:213–230. doi:10.1016/0022-2860(91)85029-3
- [36] Bellissent-Funel M-C, Chen SH, Zanotti J-M. Single-particle dynamics of water molecules in confined space. *Phys Rev E.* 1995;51:4558–4569. doi:10.1103/PhysRevE.51.4558
- [37] Lappi SE, Smith B, Franzen S. Infrared spectra of H(2)16O, H(2)18O and D(2)O in the liquid phase by single-pass attenuated total internal reflection spectroscopy. *Spectrochimica Acta Part A.* 2004;60:2611–2619. doi:10.1016/j.saa.2003.12.042
- [38] Toukan K, Ricci MA, Chen S-H, Loong C-K, Price DL, Teixeira J. Neutron-scattering measurements of wave-vector-dependent hydrogen density of states in liquid water. *Phys Rev A.* 1988;37:2580–2589. doi:10.1103/PhysRevA.37.2580
- [39] Schwerer O. EXFOR formats description for users (EXFOR Basics). Documentation Series for the IAEA nuclear data section. Vienna; 2008. (Report IAEA-NDS-206).
- [40] Zaitsev KN, Petrov VN, Kuznetsov SP, Langer OA, Meshkov IV, Perekrestenko AD. The total cross sections of the interaction of ultracold neutrons with H<sub>2</sub>O and D<sub>2</sub>O. *Soviet At Energy.* 1991;70(3):238–242. doi:10.1007/BF01126475